The following publication Yang, X., Wu, H., Li, Y., Kang, S., Chen, B., Lu, H., Lee, C. K. M., & Ji, P. (2020). Dynamics and Isotropic Control of Parallel Mechanisms for Vibration Isolation. IEEE/ASME Transactions on Mechatronics, 25(4), 2027–2034 is available at https://doi.org/10.1109/TMECH.2020.2996641.

Dynamics and Isotropic Control of Parallel Mechanisms for Vibration Isolation

Xiaolong Yang, Hongtao Wu, Yao Li, Shengzheng Kang, Bai Chen, Huimin Lu, *Senior Member, IEEE*, C. K. M. Lee, and Ping Ji

***Abstract*—Parallel mechanisms have been employed as the architectures of high-precision vibration isolation systems. However, their performances in all DOFs are nonidentical. The conventional solution to this problem is isotropic mechanism design, which is laborious and can hardly be achieved. This paper proposes a novel concept, namely isotropic control, to solve this problem. The dynamic equations of parallel mechanisms with base excitation are established and analyzed. The isotropic control framework is then synthesized in the modal space. We derive the explicit relationship between the modal control force and the actuation force in joint space, enabling the implementation of the isotropic controller. The multi-DOF system is transformed into multi identical single-DOF systems. Under the framework of isotropic control, the parallel mechanisms obtain an identical frequency response for all modes. An identical corner frequency, active damping, and rate of low-frequency transmissibility are achieved for all modes using a combining proportional, integral, and double integral compensator as the sub-controller. A 6-UPS parallel mechanism is presented as an example to demonstrate the effectiveness of the new approach.**

***Index Terms*— Dynamics, isotropic control, parallel mechanism, vibration isolation**

I. Introduction

Multi-dimensional vibration isolation is indispensable for high-precision requirements in space and ground applications, e.g., microscopes and interferometers, which work in a super-quiet environment [1–2]. Parallel mechanisms possess the advantages of high precision and high bandwidth compared to their serial counterparts [3–4]. With active vibration control techniques [5–6], they can serve as the fundamental architectures of multi-dimensional vibration isolation platforms [7–9].

This work was supported in part by the National Key Research and Development Program of China under Grant 2018YFC0309100 and in part by the National Natural Science Foundation of China under Grant 51975277. (Corresponding author: Xiaolong Yang.)

X. Yang, H. Wu, Y. Li, S. Kang and B. Chen are with College of Mechanical and Electrical Engineering, Nanjing University of Aeronautics and Astronautics, 29 Yudao Street, Nanjing 210016 China (e-mail: yang_xiaolong@nuaa.edu.cn; meehtwu@nuaa.edu.cn; liyaokkx@nuaa.edu.cn; kangsz@nuaa.edu.cn; chenbye@nuaa.edu.cn).

H. Lu is with the Department of Mechanical and Control Engineering, Kyushu Institute of Technology, Kitakyushu 804-8550, Japan (email: dr.huimin.lu@ieee.org).

C. K. M. Lee and P. Ji are with the Department of Industrial and Systems Engineering, The Hong Kong Polytechnic University, Hong Kong (email: ckm.lee@polyu.edu.hk; p.ji@polyu.edu.hk).

However, the dynamic characteristics of multi-DOF parallel mechanisms are anisotropic, i.e., various natural frequencies and damping ratios for various DOFs [11–20]. The anisotropic characteristics cause nonidentical performances in various modes [10–11]. To address this problem, the researchers focused on the isotropic design of parallel mechanisms to achieve an identical motion characteristic in all DOFs [10–20]. Allais *et al*. [12] conducted kinematic isotropic design for parallel mechanisms with even kinematic chains. Yun *et al*. [13] developed a kinematic isotropic Stewart platform for telescope secondary mirror. Li et al. [14] optimized a six-axis vibration isolator using a novel kinematic isotropic index. Based on kinematic isotropy, a decoupled dynamics and control in task space was obtained [15]. Jiang *et al*. [16–17] and He *et al*. [18] researched the dynamic isotropic design of the Stewart parallel platforms. Wu et al. [19] carried out a detailed dynamic isotropic design of the Stewart platform, considering the mass of kinematic chains. However, the complete isotropy has not been achieved in their designs. For the Stewart platform with a free-floating base, Yang *et al*. [20] obtained the design criteria of complete dynamic isotropy. These design criteria imposed substantial constraints on the geometry, mass and inertia. Since parallel mechanisms contain multi closed loops, resulting in complicate kinematics and dynamics [21-23], the solution to the complete dynamic isotropy can hardly be achieved. Moreover, isotropic design results in a rather complicated mechanical implementation even if the dynamics of kinematic chains were excluded.

In this paper, we propose to achieve isotropic performance from a control perspective for the first time. Although the parallel mechanisms have strong coupling in joint space and task space, they can be decoupled in modal space [24–26]. And thus, it is available to tune the performances to be identical in modal space independently. The dynamics of the parallel mechanisms were widely researched when the base was treated as fixed [26–27]. Since the base is excited by external disturbances for vibration isolation, in this paper, we will establish the dynamics of the parallel mechanisms with base movement and analyze the dynamics in modal space. Various control algorithms have been developed for active vibration isolation, including robust control [28], robust and optimal control [29] feedforward control [30], etc. These algorithms are effective in vibration control for certain issues but not able to solve the anisotropic problem of parallel mechanisms. A new control framework will be synthesized in modal space to

achieve the isotropic performance of vibration isolation. We will reveal the explicit relation between the modal control forces and the actuation forces in joint space, facilitating the implementation of the controller. The control parameters in all sub-controller channels are adjusted simultaneously to achieve the isotropic performance of vibration isolation for all modes.

The contributions of this paper include: (1) An isotropic control framework is proposed to obtain an isotropic performance of vibration isolation for parallel mechanisms; (2) The dynamic equations of parallel mechanisms with base excitation are established and analyzed in modal space; (3) Under the isotropic control framework, a combining proportional, integral, and double integral compensator is employed in every sub-controller channel to achieve an identical corner frequency, active damping and rate of low-frequency transmissibility for all modes.

The remainder of this paper is organized as follows. In Section II, the dynamics of parallel mechanisms is researched, and the problem of anisotropy is discussed. The synthesis and analysis of the isotropic controller are presented in Section III. The simulation results and experiment validation are provided in Section IV and V, respectively. The conclusions are summarized in Section VI.

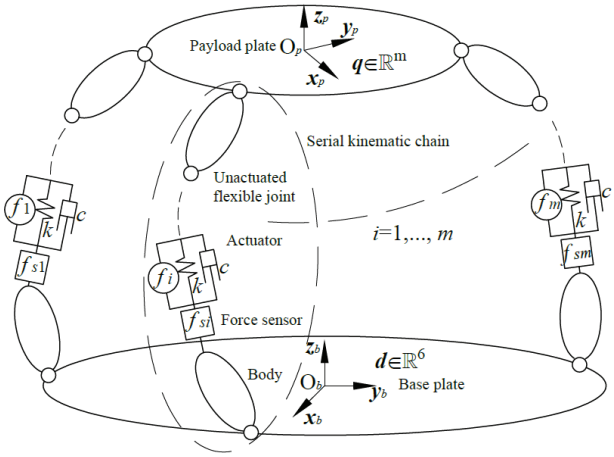

Fig. 1 A general parallel mechanism for multi-DOF vibration isolation. It is composed of a base plate, a payload plate and series kinematic chains connecting the base and the payload. A collocated actuator/ sensor pair is used in each kinematic chain. The mechanism isolates the disturbances to be transmitted from the base plate to the payload plate.

II. Dynamics of Parallel Mechanisms

This section discusses the dynamics and the anisotropic problem of the parallel mechanisms. Fig. 1 depicts a general parallel mechanism for multi-DOF vibration isolation. It is composed of a base plate, a payload plate and serial kinematic chains connecting the base and the payload. The payload plate supports the sensitive equipment. The kinematic chains can be selected as 6-UPS, 6-PUS, 3-RPS, 3-UPU, etc., which depend on the requirement of degrees of freedom.

A. Modeling General Parallel Mechanisms with Base Excitation

Let us assume the parallel mechanism possess m ($m \le 6$) DOFs with m kinematic chains. The actuator is an active prismatic joint, modeled as a spring and damper in parallel with a source of force. The collocated force sensor measures the output force of the actuator:

$$\mathbf{f}_s = \mathbf{f} - k\mathbf{l} - c\dot{\mathbf{l}}. \tag{1}$$

$\mathbf{f}_s$, $\mathbf{f}$, and $\mathbf{l}$ denote the vectors composed of the displacements, velocities, and applied forces of the actuators, respectively. k and c denote the actuators' stiffness and damping, respectively.

Let $\mathbf{q} \in \mathbb{R}^m$ represent the independent coordinates for parameterizing the pose of the payload plate apart from the equilibrium configuration. The base plate is free floating and excited by six-DOF disturbances, denoted by $\mathbf{d}$.

There exist linear relations at the the equilibrium configuration [20]:

$$\dot{\mathbf{l}} = \mathbf{J}_{lq}\dot{\mathbf{q}} - \mathbf{J}_{lb}\dot{\mathbf{d}}, \mathbf{l} = \mathbf{J}_{lq}\mathbf{q} - \mathbf{J}_{lb}\mathbf{d}. \tag{2}$$

$\mathbf{J}_{lq}$ is the Jacobian matrix of the mechanism. $\mathbf{J}_{lb}$ is a liner transformation between $\dot{\mathbf{l}}$ and the twist of the base plate. Likewise, the twist of each body can be written as

$$\mathbf{t}_i = \mathbf{J}_{iq}\dot{\mathbf{q}} - \mathbf{J}_{ib}\dot{\mathbf{d}} \ \ (i = 1, \cdots n). \tag{3}$$

n is the amount of the bodies of the mechanism excluding the base plate. $\mathbf{J}_{iq}$ is a linear map from $\dot{\mathbf{q}}$ to the twist of the i^{th} body, denoted by $\mathbf{t}_i$. $\mathbf{J}_{iq}$ is the partial velocity and partial angular velocity matrix of the i^{th} body in terms of Kane's method.

The dynamics of the parallel mechanism with base excitation can be written as [26]

$$\begin{aligned} &\mathbf{M}\ddot{\mathbf{q}} + \mathbf{D}\dot{\mathbf{q}} + \mathbf{K}\mathbf{q} = \mathbf{J}_{lq}{}^{\mathrm{T}}\mathbf{f} + \mathbf{A}\dot{\mathbf{d}} + \mathbf{B}\mathbf{d}, \\ &\mathbf{M} = \sum_{i=1}^{n} \mathbf{J}_{iq}{}^{\mathrm{T}} \begin{pmatrix} \mathbf{I}_i & \\ & m_i\mathbf{E}^{3\times 3} \end{pmatrix} \mathbf{J}_{iq}, \mathbf{D} = c\mathbf{J}_{lq}{}^{\mathrm{T}}\mathbf{J}_{lq}, \\ &\mathbf{K} = k\mathbf{J}_{lq}{}^{\mathrm{T}}\mathbf{J}_{lq}, \mathbf{A} = c\mathbf{J}_{lq}{}^{\mathrm{T}}\mathbf{J}_{lb}, \mathbf{B} = k\mathbf{J}_{lq}{}^{\mathrm{T}}\mathbf{J}_{lb}. \end{aligned} \tag{4}$$

m_i and $\mathbf{I}_i$ denote the mass and inertia of the i^{th} body, respectively. $\mathbf{E}^{3\times 3}$ is the 3×3 identical matrix. $\mathbf{A}\dot{\mathbf{d}} + \mathbf{B}\mathbf{d}$ is the disturbance force induced by the movement of the base plate.

Note that for the parallel mechanisms discussed in this paper, the damping $\mathbf{D}$ is always proportional to the stiffness matrix $\mathbf{K}$ because the damping and stiffness are both induced by the actuators. Thus, the matrices $\mathbf{M}$, $\mathbf{D}$, $\mathbf{K}$ can be diagonalizable simultaneously:

$$\begin{aligned} &\mathbf{\Phi}^{\mathrm{T}}\mathbf{M}\mathbf{\Phi} = \mathbf{E}^{m\times m}, \mathbf{\Phi}^{\mathrm{T}}\mathbf{D}\mathbf{\Phi} = \frac{c}{k}\mathbf{\Omega}^2, \\ &\mathbf{\Phi}^{\mathrm{T}}\mathbf{K}\mathbf{\Phi} = \mathbf{\Omega}^2, \mathbf{\Omega} = \mathbf{diag}\left(\omega_1, \cdots, \ \omega_m\right) \end{aligned}, \tag{5}$$

where $\mathbf{E}^{m\times m}$ is an m×m identity matrix, $\omega_i (i = 1, \cdots, m)$ are the natural frequencies of the mechanism, and $\mathbf{\Phi} \in \mathbb{R}^{m\times m}$ is composed of the mode shapes corresponding to distinct natural frequencies.

Let us transform the dynamics from tasks space to modal space to perform the dynamic analysis conveniently:

$$\mathbf{q} = \mathbf{\Phi}\mathbf{q}_\Phi, \tag{6}$$

where $\mathbf{q}_\Phi = (q_{\Phi 1}, \cdots, q_{\Phi m})^{\mathrm{T}}$ is the vector composed of modal amplitudes.

Define the control force and the disturbance in the modal space, denoted as $\mathbf{d}_\Phi$ and $\mathbf{f}_\Phi$ respectively:

$$\mathbf{d} = \mathbf{J}_{lb}(q_0)^{-1}\mathbf{J}_{lq}(q_0)\boldsymbol{\Phi}\mathbf{d}_\Phi,\ \mathbf{f}_\Phi = \boldsymbol{\Phi}^{\mathrm{T}}\mathbf{J}_{lq}^{\mathrm{T}}\mathbf{f}. \quad (7)$$

Left multiplying by $\boldsymbol{\Phi}^{\mathrm{T}}$, and considering (5), (6), and (7), the dynamic equation (4) turns into the decoupled equation:

$$\ddot{\mathbf{q}}_\Phi + \frac{c}{k}\boldsymbol{\Omega}^2\dot{\mathbf{q}}_\Phi + \boldsymbol{\Omega}^2\mathbf{q}_\Phi = \mathbf{f}_\Phi + \frac{c}{k}\boldsymbol{\Omega}^2\dot{\mathbf{d}}_\Phi + \boldsymbol{\Omega}^2\mathbf{d}_\Phi. \quad (8)$$

In the following of this paper, (8) will be used for the control synthesis and performance analysis of the mechanism to avoid its strong coupling effects in physical space, e.g., the workspace and joint space.

B. Problem of Anisotropy

In this subsection, we will discuss the dynamic performance of the mechanism with the commonly used decentralized controller to illuminate the ubiquitous anisotropy. Fig. 2 depicts the control block diagram of the decentralized control framework. Zero force tracking is employed to achieve the performance of vibration isolation. The sub-controller $H(s)$ can be designed with various control algorithms, but the control gains are the same in all channels.

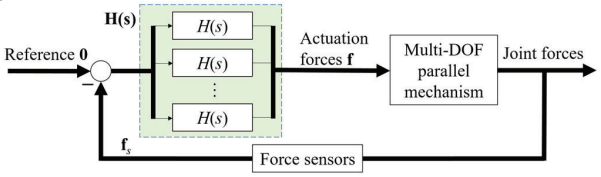

Fig. 2 Decentralized control framework. The sub-controller $H(s)$ can be designed with various control algorithms, and the control gains are the same in all channels.

Each actuator has an independent control input:

$$\mathbf{f} = -H(\mathrm{s})\mathbf{f}_s. \quad (9)$$

Substituting (1) into (9), we obtain

$$\mathbf{f} = \frac{H(s)}{1+H(s)}\left(k(\mathbf{l}-\mathbf{l}_0)+c\dot{\mathbf{l}}\right). \quad (10)$$

Considering (2), (7) and (10), (8) turns into

$$\begin{aligned}\ddot{\mathbf{q}}_\Phi + \frac{1}{1+H(s)}\frac{c}{k}\boldsymbol{\Omega}^2\dot{\mathbf{q}}_\Phi + \frac{1}{1+H(s)}\boldsymbol{\Omega}^2\mathbf{q}_\Phi \\ = \frac{1}{1+H(s)}\frac{c}{k}\boldsymbol{\Omega}^2\dot{\mathbf{d}}_\Phi + \frac{1}{1+H(s)}\boldsymbol{\Omega}^2\mathbf{d}_\Phi\end{aligned}. \quad (11)$$

Applying the Laplace transform, we obtain the frequency response function of the transmissibility between the disturbance displacement $d_{\Phi i}$ and the payload displacement $q_{\Phi i}$:

$$\frac{q_{\Phi i}}{d_{\Phi i}} = \frac{(c/k)\omega_i^2 s + \omega_i^2}{(1+H(s))s^2 + (c/k)\omega_i^2 s + \omega_i^2}\ (i = 1, \cdots, m) \quad (12)$$

Unless the natural frequencies of all the modes are identical, i.e., dynamic isotropic design, the sub-controller $H(\mathrm{s})$ leads to different pole locations for the various modes, i.e., the anisotropic performance. To illustrate, we use an integral compensator to obtain active damping for the various modes:

$$H(s) = g_{\mathrm{I}}/s. \quad (13)$$

Substituting (13) into (12), we obtain the active damping ratios for the various modes:

$$\zeta_{ai} = g_{\mathrm{I}}/(2\omega_i) + (c/2k)\omega_i \quad (i = 1, \cdots, m). \quad (14)$$

Taking the 6-UPS parallel mechanism [26] as an example, we observe its response under open loop ($g_{\mathrm{I}} = 0$) and closed loop ($g_{\mathrm{I}} = 300$), respectively. The natural frequencies are 115, 115, 83, 82, 42, and 42 Hz, respectively. Fig. 3 depicts the frequency response of the six modes. The six active damping ratios turn into 0.220, 0.220, 0.295, 0.300, 0.572 and 0.572, which are obviously not identical. The mechanism cannot obtain an isotropic performance unless the six natural frequencies are identical. From a perspective of mechanical design, one can achieve an isotropic performance in all DOFs by adjusting the mass, inertia, and geometry of the mechanism, i.e., **M**, **D**, **K** in (4), which requires a rather complicated design process.

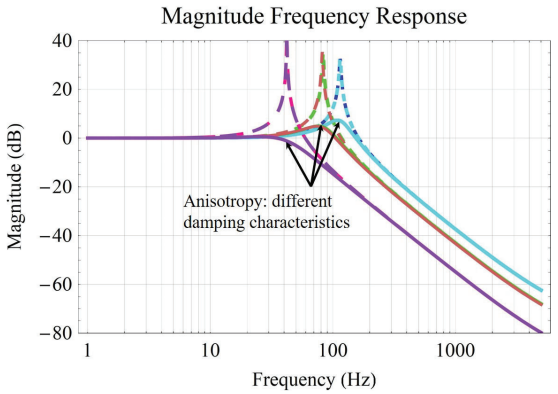

Fig. 3 Magnitude frequency response of the transmissibility between the disturbance displacement and the payload displacement for the 6-UPS parallel mechanism [26] within the decentralized control framework. The dashed lines represent the open-loop responses. The continuous lines represent the closed-loop responses. The modes with different natural frequencies have different active damping. The curves coincide for the modes with the same and slightly different frequencies. The gain g_{I} can only reach an optimal value for a certain mode or has to be adjusted to achieve a compromise in the performance for the various modes. The six active damping ratios turn into 0.220, 0.220, 0.295, 0.300, 0.572 and 0.572.

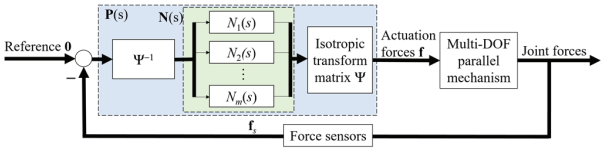

Fig. 4 The proposed isotropic control framework. The sub-controller $N_i(s)$ can be designed with various control algorithms, and the control gains in all channels are adjusted according to the various natural frequencies of the mechanism.

III. Isotropic Control of Parallel Mechanisms

In this section, we will solve the problem of anisotropy from the perspective of controller synthesis. We will reveal that the isotropic performance can be achieved by synthesizing an appropriate active control force, i.e., **f** in (4) instead of the complex and laborious mechanical design.

A. *Synthesis of the Isotropic Control Framework*

According to the above discussion, we find the reason for the anisotropic performance is that the same sub-controller $H(s)$ leads to different pole locations for the various modes with different natural frequencies. The idea to achieve an isotropic performance is to synthesize the appropriate actuation force that makes the frequency response function of the mechanism change from Eq.(12) to

$$\frac{q_{\Phi i}}{d_{\Phi i}}=\frac{(c/k)\omega_i^2 s+\omega_i^2}{(1+N_i(s))s^2+(c/k)\omega_i^2 s+\omega_i^2}\quad (i=1,\cdots,m)\,. \tag{15}$$

In (15), the sub-controllers $N_1(s)$,…, $N_m(s)$ will have different control gains associated with the various natural frequencies. Considering (8) and (15), the modal control force can be synthesized as

$$\mathbf{f}_\Phi=\left(1+\frac{c}{k}s\right)\boldsymbol{\Omega}^2\left(\mathbf{E}^{m\times m}+\mathbf{N}(s)\right)^{-1}\mathbf{N}(s)\left(\mathbf{q}_\Phi-\mathbf{d}_\Phi\right), \tag{16}$$

where $\mathbf{N}(s)=\mathbf{diag}(N_1(s),\cdots,N_m(s))$ is an m×m diagonal matrix.

On the other hand, the actuation force in the joint space is the feedback of the sensor output:

$$\mathbf{f}=-\mathbf{P}(s)\mathbf{f}_s\,. \tag{17}$$

Substituting (1) into (17), and considering (4)–(7), we obtain

$$\mathbf{f}_\Phi=\left(1+\frac{c}{k}s\right)\boldsymbol{\Omega}^2\boldsymbol{\Phi}^{-1}\mathbf{J}_{lq}^{-1}\left(\mathbf{E}^{m\times m}+\mathbf{P}\right)^{-1}\mathbf{P}\mathbf{J}_{lq}\boldsymbol{\Phi}\left(\mathbf{q}_\Phi-\mathbf{d}_\Phi\right). \tag{18}$$

Comparing (16) and (18), we get the relation between $\mathbf{P}(s)$ and $\mathbf{N}(s)$:

$$\boldsymbol{\Phi}^{-1}\mathbf{J}_{lq}^{-1}\left(\mathbf{E}^{m\times m}+\mathbf{P}\right)^{-1}\mathbf{P}\mathbf{J}_{lq}\boldsymbol{\Phi}=\left(\mathbf{E}^{m\times m}+\mathbf{N}\right)^{-1}\mathbf{N}\,. \tag{19}$$

Noting that $\mathbf{E}^{m\times m}=\mathbf{J}_{lq}\boldsymbol{\Phi}\boldsymbol{\Phi}^{-1}\mathbf{J}_{lq}^{-1}$ and $\left(\mathbf{E}^{m\times m}+\mathbf{P}\right)^{-1}\mathbf{P}=\mathbf{E}^{m\times m}-\left(\mathbf{E}^{m\times m}+\mathbf{P}\right)^{-1}$, we, fortunately, find the explicit solution of $\mathbf{P}(s)$ as

$$\mathbf{P}(s)=\mathbf{J}_{lq}\boldsymbol{\Phi}\mathbf{N}(s)\boldsymbol{\Phi}^{-1}\mathbf{J}_{lq}^{-1}. \tag{20}$$

Fig. 4 depicts the control block diagram corresponding to (17) and (20). Our proposed controller employs the matrix, $\boldsymbol{\Psi}=\mathbf{J}_{lq}\boldsymbol{\Phi}$, to transform the control laws into m independent spaces where the dynamic performance can be regulated independently to be identical. The control gains in the sub-controllers $N_m(s)$ are tuned according to the natural frequencies in various modes.

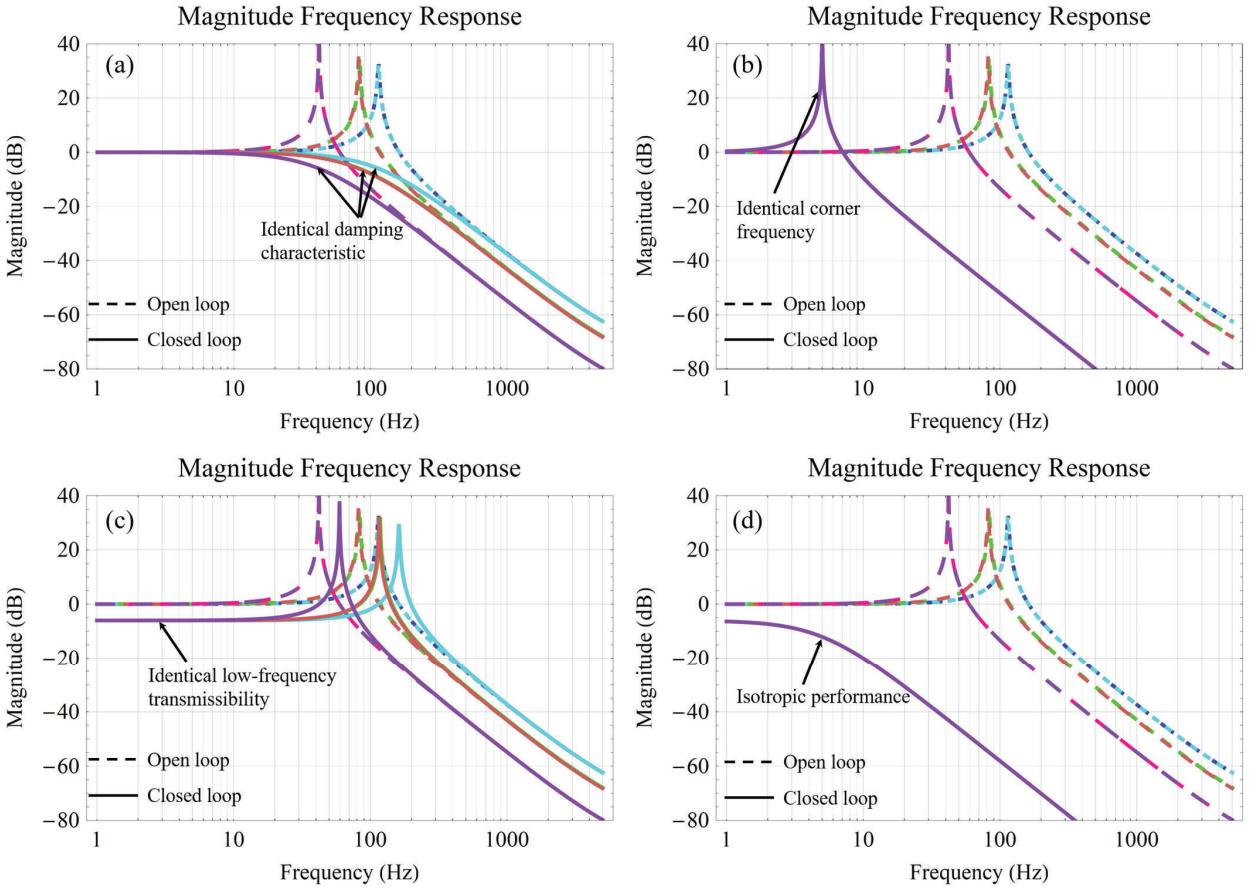

Fig. 5 Frequency response of the 6-UPS parallel mechanism within the proposed isotropic control framework. The dashed lines and continuous lines represent the open-loop and closed-loop responses, respectively. The curves coincide for the modes with the same and slightly different frequencies in the open-loop responses. (a) Identical active damping by tuning integral gains g_{Ii}. (b) Identical corner frequency, i.e., vibration isolation bandwidth, by tuning proportional gains g_{Pi}. (c) Identical rate of low-frequency transmissibility by tuning double integral gains g_{IIi}. (d) The variable modes have an isotropic performance when tuning the proportional, integral, and double integral gains simultaneously. The gains are determined by the various natural frequencies of the mechanism.

B. Isotropic Performance Analysis

To illustrate the isotropic performance of active vibration isolation, we designed $N_i(s)$ as a combining proportional, integral, and double integral compensator:

$$N_i(s) = g_{\mathrm{P}i} + \frac{g_{\mathrm{I}i}}{s} + \frac{g_{\mathrm{II}i}}{s^2} \quad (i = 1, \cdots, m). \tag{21}$$

Substituting (21) into (15), we get

$$\frac{q_{\Phi i}}{d_{\Phi i}} = \frac{(c/k)\omega_i^2 s + \omega_i^2}{(1 + g_{\mathrm{P}i})s^2 + ((c/k)\omega_i^2 + g_{\mathrm{I}i})s + (g_{\mathrm{II}i} + \omega_i^2)}. \tag{22}$$

According to (22), the rates of low-frequency transmissibility for all the modes are

$$\eta_i = \omega_i^2 / (g_{\mathrm{II}i} + \omega_i^2) \quad (i = 1, \cdots, m). \tag{23}$$

According to (22) and (23), all the corner frequencies are

$$\omega_{ci} = \omega_i / \sqrt{\eta_i (1 + g_{\mathrm{P}i})} \quad (i = 1, \cdots, m). \tag{24}$$

According to (22), (23) and (24), all the active damping ratios are

$$\zeta_{ai} = \eta_i \omega_{ci} (g_{\mathrm{I}i} / (2\omega_i^2) + c/(2k)) \quad (i = 1, \cdots, m). \tag{25}$$

According to (23), (24) and (25), we can tune the control gains to obtain an identical rate of low-frequency transmissibility, corner frequency, and active damping simultaneously for all the modes. If they are denoted as η, ω_c and ζ_a respectively, the control gains are calculated as

$$\begin{aligned} &g_{\mathrm{II}i} = \omega_i^2 (1/\eta - 1),\ g_{\mathrm{P}i} = \omega_i^2 / (\eta\omega_c^2) - 1, \\ &g_{\mathrm{I}i} = \omega_i^2 (2\zeta_a / (\eta\omega_c) - c/k) \quad (i = 1, \cdots, m) \end{aligned}. \tag{26}$$

According to (26), we observe that increasing $g_{\mathrm{II}i}$ will decrease the rate of low-frequency transmissibility η, increasing $g_{\mathrm{P}i}$ will decrease the corner frequency ω_c, and increasing $g_{\mathrm{I}i}$ will increase active damping ratio ζ_a.

Substituting (26) into (22), it is obviously that the frequency response function of the transmissibility between the disturbance displacement $d_{\Phi i}$ and the payload displacement $q_{\Phi i}$ becomes identical as

$$\frac{q_{\Phi i}}{d_{\Phi i}} = \frac{(c/k\, s + 1)\eta\omega_c^2}{s^2 + 2\zeta_c\omega_c s + \omega_c^2} \quad (i = 1, \cdots, m). \tag{27}$$

Taking the 6-UPS parallel mechanism [26] as an example, we calculate the magnitude frequency response of the transmissibility between the disturbance displacement and the payload displacement for all the six modes. When the integral gains $g_{\mathrm{I}i}$ $(i = 1, \cdots, 6)$ increase, an identical damping ratio is obtained for the six modes, as shown in Fig. 5 (a). When the proportional gains $g_{\mathrm{P}i}$ $(i = 1, \cdots, 6)$ increase, an identical corner frequency is obtained, implying the six modes have the same bandwidth of vibration isolation, as shown in Fig. 5 (b). Fig. 5(c) depicts an identical rate of low-frequency transmissibility when the double integral gains $g_{\mathrm{II}i}$ $(i = 1, \cdots, 6)$ increase. The identical active damping, corner frequency, and rate of low-frequency transmissibility are achieved simultaneously for all modes when we use a combining proportional, integral, and double integral compensator as the sub-controller, as shown in Fig. 5 (d).

C. Stability Analysis

The stability was associated with the location of the poles of the system in the left half plane. According to (27), the closed-loop poles of the variable modes are

$$p_i = -\zeta_a\omega_c \pm \omega_c\sqrt{\zeta_a^2 - 1} \quad (i = 1, \cdots, m). \tag{28}$$

From (28), we see that the system is always stable as long as the control gains are positive. The root locus for the closed-loop poles of this system is shown in Fig. 6. It is seen that increasing the proportional gain $g_{\mathrm{P}i}$ makes the closed-loop poles move towards the imaginary axis, decreasing the stability margin. Fortunately, increasing the integral gain $g_{\mathrm{I}i}$ pushes these poles deeper to the left half plane, increasing the stability. Increasing the double integral gain $g_{\mathrm{II}i}$ makes the poles apart from the real axis, and thus does not affect the stability.

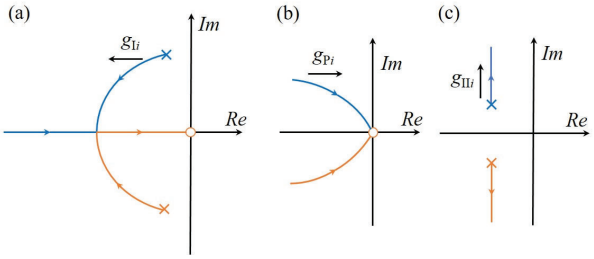

Fig. 6 Root locus of the mechanism with P+I+II control algorithm within the isotropic control framework. (a) Increasing the integral gain $g_{\mathrm{I}i}$ pushes the poles deeper to the left half plane. (b) Increasing the proportional gain $g_{\mathrm{P}i}$ makes the poles move towards the imaginary axis. (c) Increasing the double integral gain $g_{\mathrm{II}i}$ makes the poles apart from the real axis.

D. Discussion of Isotropic Control and Isotropic Design

If the mechanism is of dynamic isotropy in terms of the mechanical structure, i.e., the multi natural frequencies are identical, the matrix $\boldsymbol{\Psi}$ will be an m×m identity matrix. And the control gains $g_{\mathrm{I}i}$, $g_{\mathrm{II}i}$ and $g_{\mathrm{P}i}$ $(i = 1, \cdots, m)$ in the multiple sub-controller $N_i(s)$ will be identical as well. In this situation, the isotropic control framework (Fig. 4), degenerates to the decentralized control framework (Fig. 2).

The benefit of the isotropic control is that it dramatically reduces the difficulty of realizing the isotropic performance. We calculate the matrix $\boldsymbol{\Psi}$ while avoiding the substantial constraints on the geometry and mass distribution. If the payload changes, we only need to update $\boldsymbol{\Psi}$ and the control gains instead of implementing a new process of mechanical design. It should be noted that an excellent mechanical design is still required. We need to guarantee the equilibrium configuration is far from singularities at the design stage such that the stiffness matrix $\mathbf{K}$ is positive definite and well-conditioned.

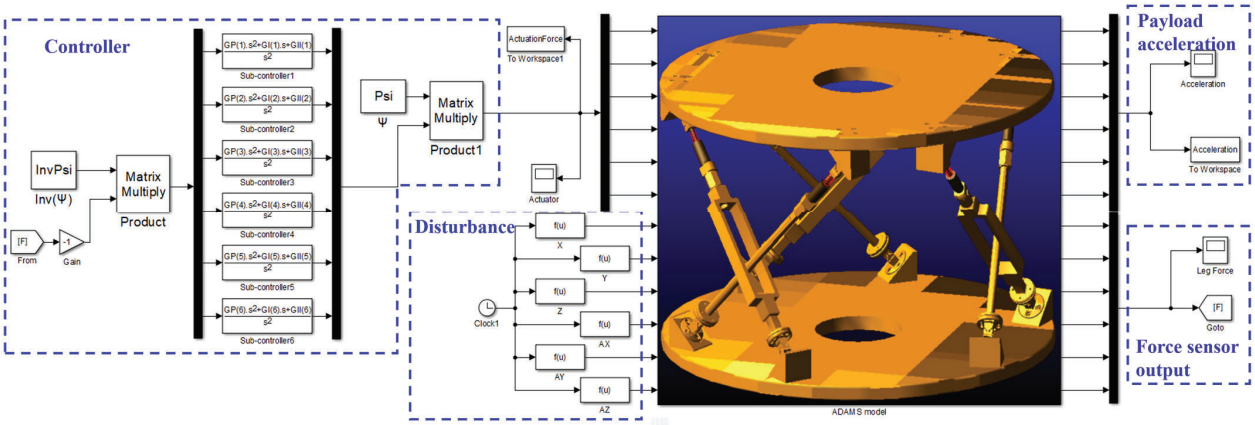

Fig. 7 ADAMS-MATLAB co-simulation model of the 6-UPS parallel mechanism. The base plate is disturbed by a six-dimensional acceleration as the input of the ADAMS model. The ADAMS model output the measurements of the force sensors and the six-dimensional acceleration of the payload plate. The isotropic control algorithm is implemented in MATLAB/Simulink to provide the actuation force for the six actuators.

Essentially, the isotropic control achieves the isotropic performance through exerting the active forces into the system, which are related to the system modes. The isotropic design endows the system with an inherent isotropic property. Thus, the isotropic control is only applicable to active vibration isolation systems, whereas the isotropic design applies to both active and passive systems.

IV. Simulation Results

We simulate to observe the performance of the isotropic control in the time domain. Fig. 7 depicts the ADAMS-MATLAB co-simulation model of the 6-UPS parallel mechanism. The base plate is disturbed by a six-dimensional acceleration. ADAMS model outputs the six actuation forces and the six-dimensional acceleration of the payload plate. The control algorithm is implemented in MATLAB/Simulink, where the feedback is the actuation forces from ADAMS model. We compare the acceleration responses of the payload in the open-loop mode and the closed-loop mode to evaluate the vibration isolation performance of the system.

The mechanism has six vibration modes with the natural frequencies of 42, 42, 80, 81, 110, and 110 Hz. We define a linear swept-frequency sine signal as the acceleration disturbance. The frequency of disturbance increases linearly from 0 to 200 Hz within 1 second to contains all the natural frequencies of the mechanism. Each component of linear-acceleration disturbance is $0.1\times\sin(2\pi\times 200t\times t)$ m/s^2, and each component of angular-acceleration disturbance is $0.1\times\sin(2\pi\times 200t\times t)$ rad/s^2.

TABLE 1 Control Gains for $\eta = 0.5$, $\omega_c = 5$Hz and $\zeta_a = 1$

Gain	Chanel 1	Chanel 2	Chanel 3	Chanel 4	Chanel 5	Chanel 6
$g_{\mathrm{II}i}$	5.187 ×10^4	5.187 ×10^4	2.737 ×10^4	2.655 ×10^4	6.989 ×10^3	6.989 ×10^3
$g_{\mathrm{P}i}$	1.050 ×10^3	1.050 ×10^3	5.537 ×10^2	5.371 ×10^2	1.406 ×10^2	1.406 ×10^2
$g_{\mathrm{I}i}$	6.461 ×10^4	6.460 ×10^4	3.381 ×10^4	3.278 ×10^4	8.370 ×10^3	8.370 ×10^3

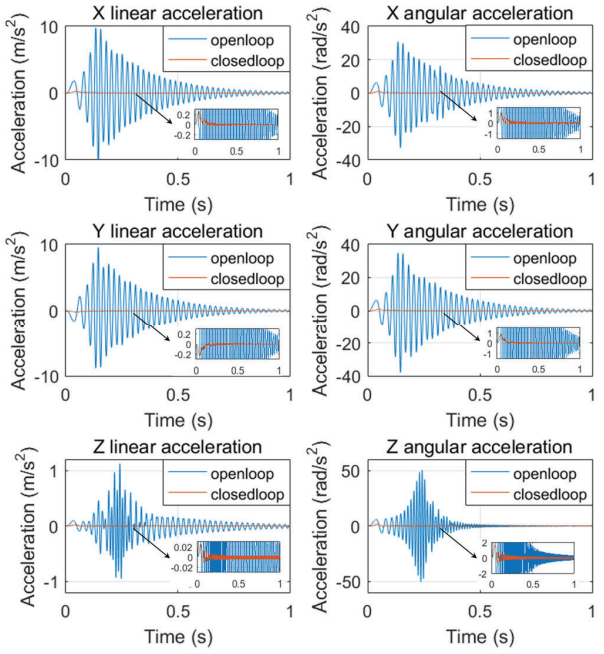

Fig. 8 Six-dimensional acceleration of the payload plate in the open-loop and closed-loop modes, respectively. The base plate is disturbed by a swept-frequency acceleration, increasing linearly from 0 to 200 Hz. Under the open-loop mode, the magnitude of the acceleration of the payload plate is amplified to the maximum at the natural frequencies. Under the closed-loop mode, the magnitude of the acceleration is attenuated throughout all frequencies.

The isotropic matrix $\boldsymbol{\Psi}$ for the 6-UPS mechanism in Fig. 7 is obtained theoretically. We derive all the matrices in (4) using the parameters from the CAD model, whose values are referenced in [26]. If we set the rate of low-frequency transmissibility $\eta = 0.5$, the corner frequency $\omega_c = 5$Hz, and the active damping ratio $\zeta_a = 1$ for all the six vibration modes, the control gains can be calculated according to (26) and are listed in Table 1. Fig. 8 depicts the acceleration response of the payload plate in the time domain without and with the control laws when the base plate is disturbed. Under the open-loop mode, the magnitude of the acceleration of the payload plate

reaches the maximum as the frequency of disturbance approaches the natural frequencies. Under the closed-loop mode, the magnitude of the acceleration of the payload plate is attenuated throughout all frequencies. ADAMS-MATLAB co-simulation presents the vibration isolation performance of the proposed method, which will be further validated by the experiment implemented in the next section.

V. Experimental Validation

The experimental setup is established, as shown in Fig. 9. The 6-UPS parallel mechanism is hung by the steel cables to compensate for its gravity. In each kinematic chain, the piezoelectric actuator can produce push and pull forces. The force sensor can measure the dynamic interaction force transmitted from the base plate to the payload plate. An external shaker disturbs the base plate of the parallel mechanism in the lateral direction. The triaxial accelerometers are assembled onto the payload plate and the base plate to measure their acceleration, respectively.

The real-time control system is implemented using MATLAB/Simulink Real-Time. **Two pieces of NI PCI-6229 Board are adopted for signal acquisition and voltage output**. The signal conditioner supplies power for the sensors and eliminates the bias of the signals. The signals of the accelerometers and force sensors are acquired into the NI PCI-6229 Board. The force data are used as feedback in the control loop. The acceleration data are used to evaluate the performance of vibration isolation. The output values of the NI PCI-6229 Board is amplified 12 times higher through the voltage amplifier and then input into the piezoelectric actuators. **The sampling rate is set at 10 kHz.** A high-pass filter at 1 Hz and a low-pass filter at 600 Hz are built digitally to limit the bandwidth of the controller and to isolate the controller from the high-frequency disturbances and low-frequency wandering signals.

The accelerations of the payload and base plates are measured under the open-loop and closed-loop modes, respectively. **The data are collected every 10 Hz from 20 Hz to 500 Hz**. The acceleration transmissibility has multi resonance peaks, as shown in **Fig. 10**. **Comparing the open-loop and closed-loop responses, we can observe that the resonances at 90 Hz, 130 Hz, and 310 Hz are attenuated, indicating the active damping is achieved.** For instance, for the first resonance peak, the closed-loop controller attenuates the magnitude of the transmissibility ratio from 24 dB to 11dB. **The rate of low-frequency transmissibility is reduced from 20 Hz to 40 Hz. It indicates the rate of low-frequency transmissibility is reduced. All the corner frequencies movie toward the left, demonstrating increased isolation bandwidth. For instance, the first corner frequency is reduced from 90 Hz to 70 Hz**. The limitation of the proposed isotropic control is the neglect of the spring dynamics of the flexible joints, which arouse resonances at higher frequencies. Fortunately, the controller is effective for the vibrations below 300 Hz, which is within the output capacity of the actuators. The mechanism has a better capacity of vibration isolation for higher frequency disturbances than the lower ones. **Fig. 11 depicts the acceleration response of the payload plate under the open-loop mode and closed-loop mode in time domain, respectively: (a) 20 Hz; (b) 90 Hz; (c) 130 Hz; (d) 310 Hz. Theoretically, increasing the proportional, integral, and double integral gains can further attenuate the vibrations. However, in practice, gradually increasing the gains causes saturation of the piezoelectric actuators. The reason is that we did not compensate the nonlinear effects of the actuators, i.e., hysteresis, which will be carried out in our future study.**

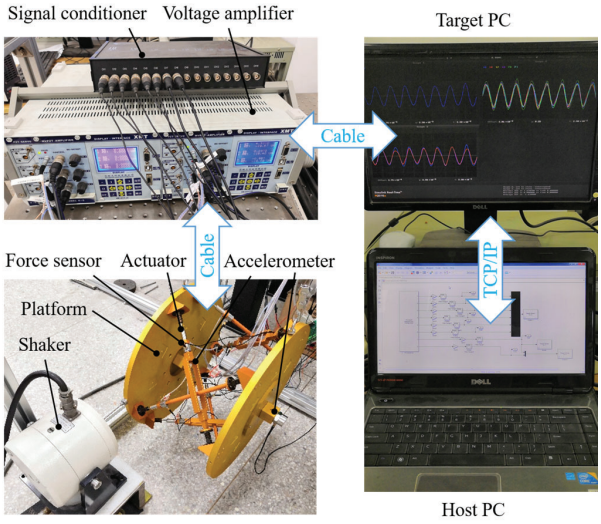

Fig. 9 Experimental setups of the 6-UPS parallel mechanism. The real-time control system is implemented using MATLAB/Simulink Real-Time.

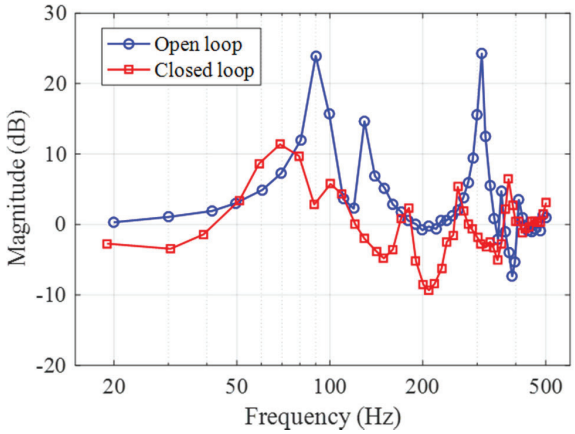

Fig. 10 Frequency response of the acceleration transmissibility from the base plate to the payload plate. The low-frequency transmissibility ratio decreases, the resonances are attenuated, and the corner frequencies move toward the left. They indicate reduced low-frequency transmissibility ratio, active damping, and increased isolation bandwidth, respectively.

VI. Conclusion

This paper proposes an isotropic control framework for the parallel mechanisms. The isotropic controller is a counterpart of the isotropic design to achieve an isotropic performance for the parallel mechanisms. If the isotropic design is guaranteed, the isotropic control will degenerate into the traditional

decentralized control. Isotropic control is more efficient than isotropic design since it only requires the update of control gains instead of a new round of mechanical design if a payload condition is changed. Both the simulation and the experimental results demonstrate effective vibration isolation capabilities of the system. Besides the proportional, integral, and double integral compensator used in this paper, other control algorithms can be implemented in the isotropic control framework to improve the vibration control performance further.

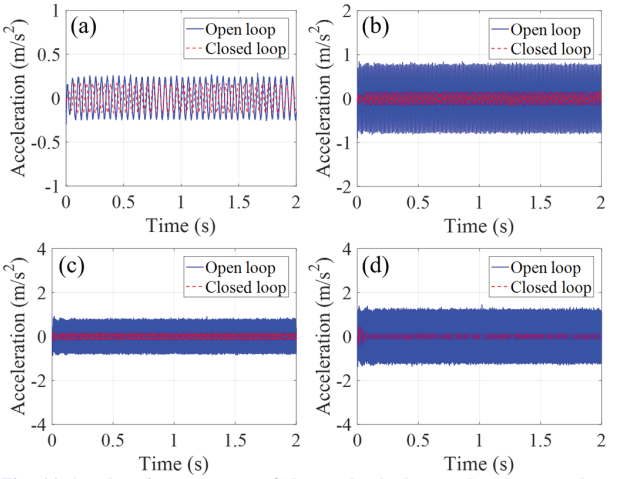

Fig. 11 Acceleration response of the payload plate under the open-loop mode and closed-loop mode in time domain, respectively: (a) 20 Hz; (b) 90 Hz; (c)130 Hz; (d) 310 Hz. As the disturbance frequency increases, the acceleration transimissibility ratio decreases. The mechanism has a better capacity of vibration isolation for higher frequency disturbances than the lower ones.

REFERENCES

[1] A. Preumont, Vibration control of active structures: an introduction: Springer Science & Business Media, 2012.

[2] C. Liu, X. Jing, S. Daley, and F. Li, "Recent advances in micro-vibration isolation," Mechanical Systems and Signal Processing, vol. 56, pp. 55-80, 2015.

[3] D. Zhang, P. Li, J. Zhang, H. Chen, K. Guo, and M. Ni, "Design and Assessment of a 6-DOF Micro/Nanopositioning System," IEEE/ASME Transactions on Mechatronics, vol. 24, no. 5, pp. 2097-2107, 2019.

[4] F. Chen, W. Dong, M. Yang, L. Sun, and Z. Du, "A PZT Actuated 6-DOF Positioning System for Space Optics Alignment," IEEE/ASME Transactions on Mechatronics, 2019.

[5] M. Rushton, H. Jamshidifar, and A. Khajepour, "Multiaxis Reaction System (MARS) for Vibration Control of Planar Cable-Driven Parallel Robots," IEEE Transactions on Robotics, vol. 35, no. 4, pp. 1039-1046, 2019.

[6] J. Liu, Y. Li, Y. Zhang, Q. Gao, and B. Zuo, "Dynamics and control of a parallel mechanism for active vibration isolation in space station," Nonlinear Dynamics, vol. 76, no. 3, pp. 1737-1751, 2014.

[7] J. E. McInroy, and J. C. Hamann, "Design and control of flexure jointed hexapods," IEEE Transactions on Robotics and Automation, vol. 16, no. 4, pp. 372-381, 2000.

[8] M. Hamaguchi, "Damping and transfer control system with parallel linkage mechanism-based active vibration reducer for omnidirectional wheeled robots," IEEE/ASME Transactions on Mechatronics, vol. 23, no. 5, pp. 2424-2435, 2018.

[9] Y. Yun, and Y. Li, "Design and analysis of a novel 6-DOF redundant actuated parallel robot with compliant hinges for high precision positioning," Nonlinear Dynamics, vol. 61, no. 4, pp. 829-845, 2010.

[10] B. D. Marneffe, M. Avraam, A. Deraemaeker, M. Horodinca, and A. Preumont, "Vibration isolation of precision payloads: A six-axis electromagnetic relaxation isolator," Journal of Guidance, Control, and Dynamics, vol. 32, no. 2, pp. 395-401, 2009.

[11] A. Preumont, M. Horodinca, I. Romanescu, B. De Marneffe, M. Avraam, A. Deraemaeker, F. Bossens, and A. A. Hanieh, "A six-axis single-stage active vibration isolator based on Stewart platform," Journal of Sound and Vibration, vol. 300, no. 3, pp. 644-661, 2007.

[12] A. A. Allais, J. E. McInroy, and J. F. O'Brien, "Locally decoupled micromanipulation using an even number of parallel force actuators," IEEE Transactions on Robotics, vol. 28, no. 6, pp. 1323-1334, 2012.

[13] H. Yun, L. Liu, Q. Li, W. Li, and L. Tang, "Development of an isotropic Stewart platform for telescope secondary mirror," Mechanical Systems and Signal Processing, vol. 127, pp. 328-344, 2019.

[14] Y. Li, X. Yang, H. Wu, and B. Chen, "Optimal design of a six-axis vibration isolator via Stewart platform by using homogeneous Jacobian matrix formulation based on dual quaternions," Journal of Mechanical Science and Technology, vol. 32, no. 1, pp. 11-19, January 01, 2018.

[15] J. E. McInroy, J. F. O'Brien, and A. A. Allais, "Designing micromanipulation systems for decoupled dynamics and control," IEEE/ASME Transactions on Mechatronics, vol. 20, no. 2, pp. 553-563, 2015.

[16] H.-z. Jiang, Z.-z. Tong, and J.-f. He, "Dynamic isotropic design of a class of Gough–Stewart parallel manipulators lying on a circular hyperboloid of one sheet," Mechanism and Machine Theory, vol. 46, no. 3, pp. 358-374, 2011.

[17] H.-z. Jiang, J.-f. He, Z.-z. Tong, and W. Wang, "Dynamic isotropic design for modified Gough–Stewart platforms lying on a pair of circular hyperboloids," Mechanism and Machine Theory, vol. 46, no. 9, pp. 1301-1315, 2011.

[18] J.-F. He, H.-Z. Jiang, Z.-Z. Tong, B.-P. Li, and J.-W. Han, "Study on dynamic isotropy of a class of symmetric spatial parallel mechanisms with actuation redundancy," Journal of Vibration and Control, pp. 1077546311409608, 2011.

[19] Y. Wu, K. Yu, J. Jiao, D. Cao, W. Chi, and J. Tang, "Dynamic isotropy design and analysis of a six-DOF active micro-vibration isolation manipulator on satellites," Robotics and Computer-Integrated Manufacturing, vol. 49, pp. 408-425, 2018.

[20] X. Yang, H. Wu, Y. Li, and B. Chen, "Dynamic isotropic design and decentralized active control of a six-axis vibration isolator via Stewart platform," Mechanism and Machine Theory, vol. 117, pp. 244-252, 2017.

[21] F. Jafari, and J. E. McInroy, "Orthogonal Gough-Stewart platforms for micromanipulation," IEEE Transactions on Robotics and Automation, vol. 19, no. 4, pp. 595-603, 2003.

[22] X. Yang, H. Wu, Y. Li, and B. Chen, "A dual quaternion solution to the forward kinematics of a class of six-DOF parallel robots with full or reductant actuation," Mechanism and Machine Theory, vol. 107, pp. 27-36, 2017.

[23] X. Yang, H. Wu, Y. Li, S. Kang, and B. Chen, "Computationally Efficient Inverse Dynamics of a Class of Six-DOF Parallel Robots: Dual Quaternion Approach," Journal of Intelligent & Robotic Systems, vol. 94, no. 1, pp. 101-113, March 05, 2019.

[24] F. Braghin, S. Cinquemani, and F. Resta, "A new approach to the synthesis of modal control laws in active structural vibration control," Journal of Vibration and Control, vol. 19, no. 2, pp. 163-182, 2013.

[25] J.-f. He, H.-z. Jiang, and Z.-z. Tong, "Modal control of a hydraulically driven redundant actuated fully parallel mechanism," Journal of Vibration and Control, vol. 23, no. 10, pp. 1585-1592, 2015.

[26] X. Yang, H. Wu, B. Chen, S. Kang, and S. Cheng, "Dynamic modeling and decoupled control of a flexible Stewart platform for vibration isolation," Journal of Sound and Vibration, vol. 439, pp. 398-412, 2019.

[27] B. Afzali-Far, P. Lidström, and K. Nilsson, "Parametric damped vibrations of Gough–Stewart platforms for symmetric configurations," Mechanism and Machine Theory, vol. 80, pp. 52-69, 2014.

[28] Y. Li, Y. Yun, and S. Xiao, "Controller design and experimental investigation of a 3-universal-prismatic-universal compliant manipulator for active vibration isolation," Journal of Vibration and Control, vol. 21, no. 16, pp. 3218-3238, 2015.

[29] H. Jamshidifar, S. Khosravani, B. Fidan, and A. Khajepour, "Vibration decoupled modeling and robust control of redundant cable-driven parallel robots," IEEE/ASME Transactions on Mechatronics, vol. 23, no. 2, pp. 690-701, 2018.

[30] M. A. Beijen, M. F. Heertjes, J. Van Dijk, and W. B. J. Hakvoort, "Self-tuning MIMO disturbance feedforward control for active hard-mounted vibration isolators," Control Engineering Practice, vol. 72, pp. 90-103, 2018/03/01/, 2018.

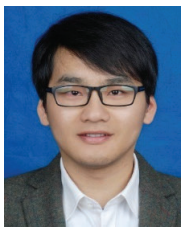

Xiaolong Yang received the B.S. degree in mechanical engineering and automation in 2011 and the M.S. and Ph.D. degrees in mechatronic engineering in 2014 and 2018, all from Nanjing University of Aeronautics and Astronautics.

From 2018 to 2019, he was a Postdoctoral Fellow and Mechatronics Laboratory Director with the Lab of Biomechatronics and Intelligent Robotics in the Mechanical Engineering Department at City University of New York, City College, US. His research interests include robotics, mechanisms and vibration control.

Hongtao Wu the M.S. degree and Ph.D. degree from Tianjin University, Tianjin, China, in 1985 and 1992, respectively, all in mechanical engineering.

In 2000, he was a Research Associate with with the Department of Industrial and Systems Engineering, The Hong Kong Polytechnic University, Hong Kong. From 2001 to 2002, he was a visiting scholar with Arizona State University. Since 1998, he has been a full professor with the College of Mechanical and Electrical Engineering at Nanjing University of Aeronautics and Astronautics. His current research interests include parallel mechanisms, robotics, and multibody system dynamics.

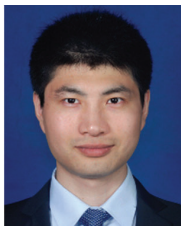

Yao Li received the B.S. degree in mechanical and electrical engineering from Shandong Agricultural University in 2012 and the M.S. degree in mechatronic engineering from Nanjing University of Aeronautics and Astronautics in 2015.

He is currently a Ph.D. candidate in mechanical and electrical engineering with Nanjing University of Aeronautics and Astronautics. His current research interests include parallel mechanisms and active vibration control.

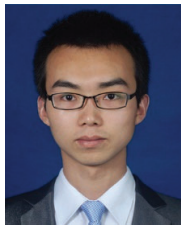

Shengzheng Kang received the B.S. degree in mechanical engineering and automation from Nanjing University of Aeronautics and Astronautics, Nanjing, China, in 2015, where he is currently working toward the Ph.D. degree in mechanical and electrical engineering.

In 2019, he was a visiting Ph.D. student with the Department of Mechanical Engineering, Chiba University in Japan. He is currently a joint Ph.D. student sponsored by the China Scholarship Council (CSC) with the Active Structures Laboratory in Department of Control Engineering and System Analysis, Université libre de Bruxelles (ULB), Brussels, Belgium. His research interests include micro/nano manipulation, parallel robots and robust control.

Bai Chen received the B.S. degree and Ph.D. degree from Zhejiang University, Hangzhou, China, in 2000 and 2005, respectively, all in mechanical engineering.

Currently, he is a full professor with the College of Mechanical and Electrical Engineering at Nanjing University of Aeronautics and Astronautics. His current research interests include minimally invasive neurosurgery robot, virtual surgery system and interventional therapy.

Huimin Lu received the B.S. degree in electronics information science and technology from Yangzhou University, Yangzhou, China, in 2008, the M.S. degrees in electrical engineering from the Kyushu Institute of Technology, Kitakyushu, Japan, and Yangzhou University, in 2011, and the Ph.D. degree in electrical engineering from the Kyushu Institute of Technology, in 2014.

From 2013 to 2016, he was a JSPS research fellow (DC2, PD, and FPD) at Kyushu Institute of Technology. Currently, he is an associate professor in Kyushu Institute of Technology, Japan and also serves as an Excellent Young Researcher of Ministry of Education, Culture, Sports, Science and Technology-Japan. He is the Fellow of European Alliance for Innovation (EAI) and Senior Member of IEEE. His research interests include computer vision, robotics, artificial intelligence, and ocean observing.

C. K. M. Lee received the B.Eng. and Ph.D. degrees from The Hong Kong Polytechnic University, Hong Kong. She is currently an Associate Professor Professor with the Department of Industrial and Systems Engineering, The Hong Kong Polytechnic University, Hong Kong. Her current research areas include logistics information management, manufacturing information systems, product development, and data mining techniques.,

Prof. Lee was the recipient of the Bronze Award of 16th China National Invention Exhibition Award in 2006 and the Outstanding Professional Service and Innovation Award of The Hong Kong Polytechnic University in 2006.

Ping Ji received the M.S. degree in manufacturing engineering from Beihang University, Beijing, China, in 1984, and the Ph.D. degree in industrial engineering from West Virginia University, Morgantown, WV, USA, in 1991.

He went to the National University of Singapore, Singapore, in 1992, and came to Hong Kong Polytechnic University, Hong Kong, in 1996. He is currently a full professor with the Department of Industrial and Systems Engineering, Hong Kong Polytechnic University, Hong Kong. His current research interests include operations management, applied optimization, and information systems.